

Comparison of the Effects of ZnO and TiO₂ on the Performance of Perovskite Solar Cells via SCAPS-1D Software Package

A. Benami^{1,*}, T. Ouslimane¹, L. Et-taya¹, A. Sohani²

¹ LM3ER-O TEA, Department of Physics, Faculty of Sciences and Techniques, Moulay Ismail University of Meknes, BP 509 Boutalamine 52000, Errachidia, Morocco

² Lab of Optimization of Thermal Systems' Installations, Faculty of Mechanical Engineering-Energy Division, K.N. Toosi University of Technology, P.O. Box: 19395-1999, No. 15-19, Pardis St., Mollasadra Ave., Vanak Sq., Tehran 1999 143344, Iran

(Received 17 January 2022; revised manuscript received 25 February 2022; published online 28 February 2022)

In the quest for a highly efficient and low-cost material for fourth-generation photovoltaic devices, organic-inorganic hybrid perovskite solar cells are gaining popularity as a new absorber. Currently, two types of solid-state perovskite device architecture are being researched. These are mesoporous and planar heterojunctions. Both structures are made up of five layers: transparent conductive oxide, electron transport material, perovskite active layer, hole transporting material, and back contact. In this work, the key characteristics of perovskite solar cells with zinc oxide (ZnO) and titanium dioxide (TiO₂) as electron transport material are simulated using the one-dimensional Solar Cell Capacitance Simulator (SCAPS-1D). TiO₂ is the most commonly used material in perovskite solar cells, but its deposition requires high temperature, which limits the commercial processing of flexible devices. ZnO is widely used in the semiconductor industry and is considered an alternative to TiO₂ due to its excellent electron transport. Simulation studies focus on the thickness, carrier diffusion length, and band gap energy of the absorber layer, which affect the photovoltaic properties of solar cell devices. The effect of working temperature is also examined. According to the findings, the use of ZnO as an electron transport material improves the cell efficiency compared to TiO₂. Because of the lower edge of the conduction band, which facilitates the transport of photogenerated electrons in a perovskite solar cell, the best efficiency got from a structure using ZnO layer is 25.40 % at ambient temperature. The simulation results show that an absorber thickness of 500 nm is appropriate for achieving high efficiency.

Keywords: Perovskite, Solar cells, Efficiency, SCAPS-1D.

DOI: [10.21272/jnep.14\(1\).01033](https://doi.org/10.21272/jnep.14(1).01033)

PACS numbers: 84.60.hj, 88.40.J –

1. INTRODUCTION

The energy received from the Sun is the most abundant type of energy sources among renewable energy resources. Every two minutes, the Earth receives energy from the Sun, equivalent to the total annual energy consumption of mankind. One day of solar radiation can provide us 10,000 times more energy than the entire planet needs. This enormous potential can be exploited by solar cells that convert solar energy into electrical power based on the photovoltaic effect [1].

Four generations of photovoltaic technologies have emerged and been studied in search for efficient, affordable, and robust solar cell devices [2]. Fourth-generation solar cells, also known as organic-inorganic, are new materials for photovoltaic applications such as hybrid perovskite solar cells (PSCs) with a certified power conversion efficiency (PCE) of 25.5 %, that is comparable to the efficiency of c-Si and surpasses that of CdTe and CIGS [3]. They were designed to overcome the drawbacks of the previous three generations, including high production cost, lower abundance of some components, toxicity of others, and low PCE.

Hybrid organic-inorganic PSCs continue to attract the attention of the scientific community because of their unique optoelectrical properties. The key characteristics of PSCs are high absorption coefficient of about 10^5 cm^{-1} , tunable direct band gap from 1.2 to 2.67 eV, long carrier lifetime, high charge mobility,

long electron-hole diffusion lengths $> 175 \mu\text{m}$, low non-radiative Auger recombination, simple fabrication process and low cost compared to archrival – silicon solar cells [4]. Perovskite material can be used not only as an absorber in solar cells, but also in photodetectors, light-emitting diodes, and batteries.

Kojima et al. [5] reported the first PCE of less than 3 % of perovskite based $\text{CH}_3\text{NH}_3\text{PbBr}_3$ in 2006. Three years later, PCE reached 3.8 % after replacing bromine with iodine. Recent progress in PSCs has resulted in a significant rise in the PCE, achieving a certified record value of 25.5 % in 2020 [3]. However, the long-term stability of these types of solar cells hinders their commercialization. Theoretically, the maximum PCE of PSCs can be almost 31 %, which close to the Shockley-Queisser limit (33 %) [2].

Numerical simulation is a powerful tool that makes it possible to understand solar cells better, identify the main parameters that affect their performance, and design new experimental production structures. Recently, Adhikari et al. [6] reported a comparative study of halide perovskite using TiO₂ and ZnO as an electron transport material (ETM) by investigating the effects of absorber thickness, doping concentration, and ETM thickness. Raoui et al. [7] evaluated the key PSC parameters for various hole and electron transport materials and analyzed the influence of the thickness of both materials and work function on the performance of the

* a.benami@fste.umi.ac.ma

PSC. Several researchers utilized the one-dimensional Solar Cell Capacitance Simulator (SCAPS-1D) to simulate the short circuit current density (J_{sc}), fill factor (FF), PCE (η), and open-circuit voltage (V_{oc}) of PSCs. Hence, numerical simulation of MAPbI₃ as a photoactive layer was carried out using SCAPS-1D. The effect of thickness, carrier diffusion length and band gap of the active layer on cell output was investigated. The impact of operating temperatures on V_{oc} , PCE, J_{sc} and FF was also studied.

2. NUMERICAL SIMULATION

To investigate the performance of PSCs, many simulation programs are used, such as SILVACO ATLAS, wxAMPS, finite element method, SCAPS, and so on. The choice of SCAPS among these software packages in this work is motivated by the fact that the simulation results are consistent with experience [2].

SCAPS-1D software (version 3.3.0.7, University of Gent, Belgium) is used as a platform for simulation of MAPbI₃ based PSCs [2]. The simulation software focuses on solving the fundamental equations in one-dimensional space that govern charge transport in semiconductors, described below [8].

The Poisson equation, which represents the relationship between electrostatic potential and charge density in one-dimensional form, is given by:

$$\begin{aligned} \frac{dE}{dx} &= -\frac{d^2\psi}{dx^2} = \\ &= \frac{q}{\epsilon} [p(x) - n(x) + N_D^+(x) - N_A^-(x) + \rho_t(x) - n_t(x)]. \end{aligned} \quad (1)$$

Here, E is the electric field, ϵ is the dielectric constant of the semiconductor material equal to $\epsilon = \epsilon_0\epsilon_r$, where ϵ_r and ϵ_0 denote the relative permittivity and vacuum permittivity, respectively, q is the electron charge, N_A^- (N_D^+) is the density of ionized acceptors (donors), ψ is the electrostatic potential, p (n) is the hole (electron) concentration, n_t (p_t) is the trapped electron (hole) concentration, and x is the position coordinate.

The continuity equations for electrons (2) and holes (3) are written as:

$$\frac{dn_p}{dt} = G_n - \frac{n_p - n_{p0}}{\tau_n} + n_p\mu_n \frac{dE}{dx} + \mu_n E \frac{dn_p}{dx} + D_n \frac{d^2n_p}{dx^2}, \quad (2)$$

$$\frac{dp_n}{dt} = G_p - \frac{p_n - p_{n0}}{\tau_p} + p_n\mu_p \frac{dE}{dx} + \mu_p E \frac{dp_n}{dx} + D_p \frac{d^2p_n}{dx^2}, \quad (3)$$

where G_p and G_n are the hole and electron generation rates, D_p and D_n are the hole and electron diffusion coefficients given by the Einstein relation [$D_i = (kT/q)\mu_i$].

The drift and diffusion equations for electrons and holes, which describe the carrier transport, are expressed in terms of the quasi-Fermi level as

$$J_n(x) = qn\mu_n E + qD_n \frac{dn}{dx} = n\mu_n \frac{dE_{Fn}}{dx}, \quad (4)$$

$$J_p(x) = qp\mu_p E - qD_p \frac{dp}{dx} = p\mu_p \frac{dE_{Fp}}{dx}, \quad (5)$$

where E_F shows the quasi-Fermi levels, the subscripts p and n represent holes and electrons, respectively, μ_p and μ_n are the hole and electron mobilities.

3. PARAMETERS OF A SIMULATED DEVICE STRUCTURE

Currently, two kinds of solid-state PSC device architecture have been investigated. They are mesoporous and planar heterojunctions. Both structures mainly consist of five layers, i.e., transparent conductive oxide (TCO), ETM, perovskite active layer, hole transport material (HTM), and back contact.

Methylammonium lead triiodide (CH₃NH₃PbI₃ or MAPbI₃) is a cost-effective and widely used material as an absorber layer in PSCs [9]. The two structures studied in this work are solid-state planar normal heterojunction architecture glass/FTO/ETM/MAPbI₃/Spiro-OMeTAD/Au (Fig. 1). The device consists of an intrinsic MAPbI₃ sandwiched between n -type TiO₂/ZnO as ETM and p -type Spiro-OMeTAD used as HTM and protects MAPbI₃ from the external environment.

Among various ETM layers, TiO₂ is the most commonly used, but its deposition requires high temperature, limiting the commercial processing of flexible PSCs [3]. ZnO is considered an alternative ETM to replace TiO₂ due to its excellent electron transport and is widely used in the semiconductor industry. The metal counter electrode on the PSC front and back contacts is made of SnO₂:F (FTO) and Au, respectively.

The corresponding energy level diagram for each layer of the proposed PSC is shown in Fig. 1. The physical parameters and values used in the PSC simulation are summarized in Table 1, collected from previously reported works [1, 8, 10-13].

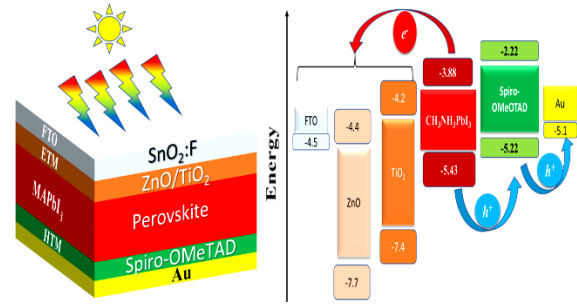


Fig. 1 – Schematic structure of the PSC device and its band alignments of constituting layers which demonstrate the main carrier transport processes

Other input parameters not included in Table 1 are: thermal velocities of holes and electrons considered are $1 \cdot 10^7 \text{ cm} \cdot \text{s}^{-1}$ [12], the energy distribution is Gaussian with a characteristic energy of 0.1 eV [13]. The electron and hole capture cross-section is $1 \cdot 10^{-15} \text{ cm}^2$, the density of states of the valence and conduction bands is $1.8 \cdot 10^{19} \text{ cm}^{-3}$ and $2.2 \cdot 10^{18} \text{ cm}^{-3}$, respectively [2, 10]. The work function of the back contact is 5.1 eV [12]. The values of series and parallel resistances are $5.6 \Omega \text{ cm}^2$ and $4202 \Omega \text{ cm}^2$, respectively [8]. The standard AM 1.5G spectrum with an incident power density of 100 mW/cm^2 is used for all simulations.

Table 1 – List of parameters used in the simulation [1, 8, 10-13]

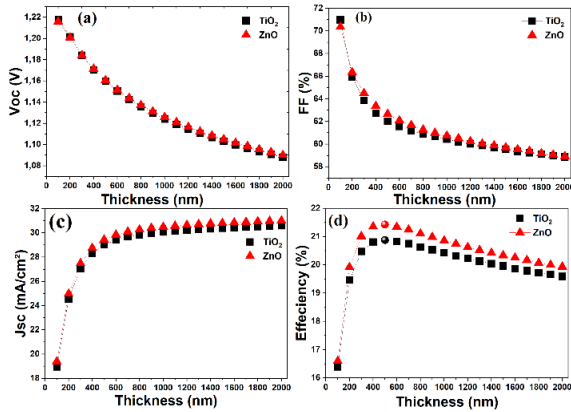
Term	Parameters	FTO	TiO ₂	ZnO	MAPbI ₃	HTM
Thickness	d (nm)	500	50	50	Variable	400
Bandgap	E_g (eV)	3.5	3.2	3.3	Variable	3
Electron affinity	χ (eV)	4	4	4	3.9	2.45
Relative permittivity	ϵ_r	9	9	9	6.5	3
Mobility of electrons/holes	μ_n/μ_p (cm ² /s)	20/10	20/10	100/25	50/50	$2 \cdot 10^{-4}/2 \cdot 10^{-4}$
Donor density	N_d (cm ⁻³)	$2 \cdot 10^{19}$	10^{16}	10^{18}	0	0
Acceptor density	N_a (cm ⁻³)	0	0	0	10^{13}	$3 \cdot 10^{18}$
Density of defects	N_t (cm ⁻³)	10^{15}	$5 \cdot 10^{15}$	10^{15}	Variable	10^{15}
Absorption coefficient	α (m ⁻¹)	From [8]	From [11]	From [8]	From [8]	From [8]

4. RESULTS AND DISCUSSION

4.1 Active Layer Thickness Optimization

In thin-film solar cells, the absorber layer plays a crucial role in determining the device performance, as it absorbs incident photons and generates charge carriers. The thickness of the active layer is one of the critical parameters that contribute to optimizing solar cell performance. It should be chosen very carefully to absorb the highest number of photons and not too large to minimize reverse saturation current.

In order to improve the performance of PSCs, the impact of the variation in the absorber thickness between 100 and 2000 nm was investigated by keeping all other device settings constant for different ETMs. Fig. 2 shows the effect of thickness variation on the performance of ETM/MAPbI₃ heterojunction solar cell, such as V_{oc} , FF, J_{sc} , and η . It can be noticed that V_{oc} and FF decrease with increasing MAPbI₃ thickness for both structures with different ETM layers, while J_{sc} raises rapidly first and then remains constant (Fig. 2c). However, the efficiency first increases to a maximum of 20.87 % and 21.42 % for 500 nm thickness, respectively, for cells with ETM layers of TiO₂ and ZnO.

**Fig. 2** – Absorber layer thickness impact on cell performance

The high PCE is due to proper band alignment between the conduction band of ETM and the conduction band of the absorber MAPbI₃, as presented in Fig. 1. Furthermore, ZnO has a higher electron mobility (100 cm²/Vs) than TiO₂ (20 cm²/Vs). As the absorber thickness increases, more photons are absorbed, then the generation of electron-hole pairs will also increase, owing to the higher absorption coefficient of MAPbI₃.

However, with a thicker absorber layer, the recombination of charge carriers within the material will increase, resulting in a decrease in efficiency. Thus, MAPbI₃ thickness of 500 nm would be the optimal value for high efficiency [14].

4.2 Influence of the Carrier Diffusion Length of the Active Layer

The properties of solar cells are significantly affected by the absorber material's quality, i.e., the carrier diffusion length, which depends on the defect density [2, 15]. For both structures, the simulated values of the diffusion lengths of electrons (L_n) and holes (L_p) are the same, since the mobility, capture cross-section, and thermal velocity of electrons and holes in the absorber are set to be the same. The effect of the carrier diffusion length of the MAPbI₃ layer, in which the carrier diffusion length corresponds to the absorber quality, was examined.

In the numerical simulation, the carrier diffusion length varied from 0.025 to 8 μ m by changing the total defect density in MAPbI₃ from $1 \cdot 10^{18}$ to $1 \cdot 10^{13}$ cm⁻³, respectively, as shown in Table 2. Fig. 3 illustrates the impact of the carrier diffusion length on the PSC photovoltaic parameter. As can be seen, all cell performance criteria are decreased when the diffusion length is less than 2 μ m. In other words, the cell performance criteria deteriorate when the total defect density in the absorber layer increases.

The strong impact of the carrier diffusion length is observed on FF, which is an essential component affecting the cell efficiency. The fill factor is as low as ~ 28 % at a diffusion length of 0.025 μ m and saturates to 60 % for a diffusion length higher than 2 μ m. Furthermore, the efficiency is severely reduced when the carrier diffusion length is less than the optimal absorber thickness of 0.5 μ m. It is because of the high recombination rate in the active layer [16].

Table 2 – Variation of carrier diffusion length for the corresponding total defect density

N_t (cm ⁻³)	10^{13}	10^{14}	10^{15}	10^{16}	10^{17}	10^{18}
L_n/L_p (μ m)	8	2.5	0.8	0.25	0.08	0.025

4.3 Effect of the Absorber Layer Band Gap

Optical absorption can be engineered by tuning the band gap energy of perovskite materials to get a device with very high performance [17]. Nonetheless, in a PSC device, band gap energy of the active layer is an

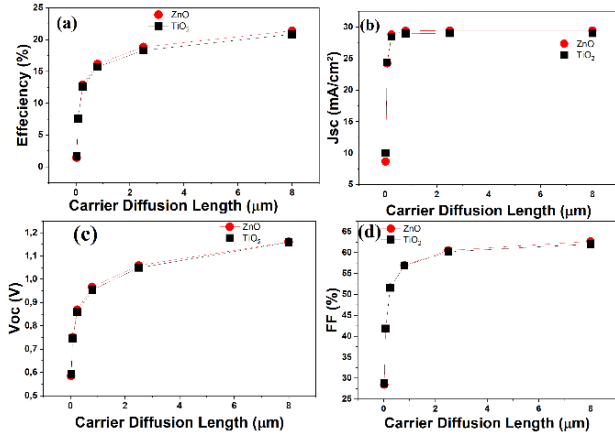


Fig. 3 – Variation of device performance with increasing carrier diffusion length

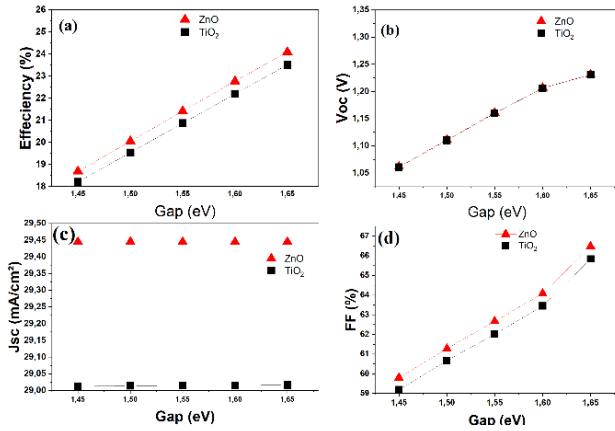


Fig. 4 – Influence of absorber band gap on device performance

important factor in optical absorption. The perfect alignment of ETM band gaps, the absorber layer, and HTM facilitates the diffusion of electrons and holes from the photoexcited MAPbI₃ layer towards the contacts and external circuit.

Previous experiments, simulations, and theoretical calculations have shown that the MAPbI₃ band gap could be tunable in the range between 1.2 and 2.67 eV [4, 18]. Here the thickness and carrier diffusion length of MAPbI₃ were set to be 500 nm and 8 μm, respectively, while other parameters were kept constant, and the band gap was changed from 1.45 to 1.65 eV. The simulated variation in device performances as a function of the absorber layer band gap is shown in Fig. 4.

It is found from Fig. 4c that J_{sc} remains almost constant with increasing band gap of the active layer, due to the increase in the optical absorption of a photon with a higher energy value exceeding the band gap of MAPbI₃. V_{oc} increases as the band gap energy increases. This happens because, after the generation of electron-hole pairs, there is a separation of excitons which reduces radiative recombination and improves the V_{oc} [19]. An increase in the fill factor due to the band gap increase is explained by the correspondence between HTM and the absorber layer. Overall, by examining the simulation results, we can deduce that as the band gap increases, the efficiency of both ETMs increases from 20.87 to 24.78 % for TiO₂ and from 21.42 to 25.40 % for ZnO.

4.4 Effect of Working Temperature

So far, room temperature has been used in all the above simulation investigations. However, solar panels operate at temperatures above 300 K because they are installed outdoors. Consequently, working temperature is a key factor in the device performance. Increased temperatures have been reported to lead to increased stress and strain in structures with growing interfacial defects, disorder, and poor interconnectivity between layers [13].

By maintaining the overall parameters constant, the effect of working temperature ranging from 300 to 440 K on the photovoltaic parameters of both structures is studied. Fig. 5 shows the influence of working temperature on the key parameters of PSCs. As expected, we notice that J_{sc} increases with temperature, owing to the energy band gap reduction and creation of a greater number of electron-hole pairs [2]. A decrease in V_{oc} as a function of operating temperature can be explained by the creation of more interfacial defects, which is accompanied by an increase in series resistance and reduction in the exciton diffusion length [13]. Besides, temperature rise also affects the hole and electron mobilities and carrier concentration, leading to a decrease in the PCE of PSCs [2, 13]. Hence, according to Fig. 5, we have achieved the best photovoltaic performances at 300 K.

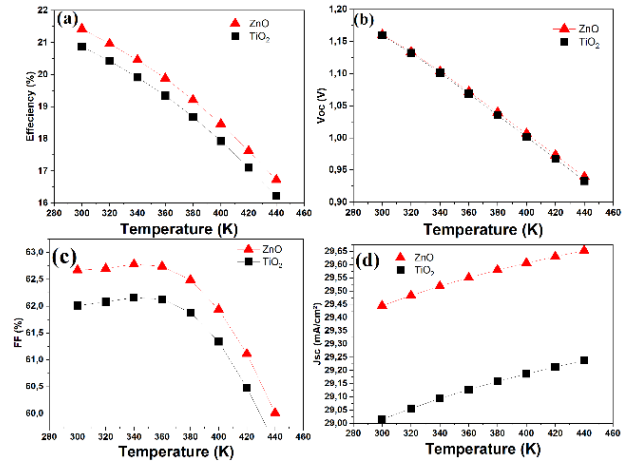


Fig. 5 – PCE, V_{oc}, FF and J_{sc} as a function of working temperature

5. CONCLUSIONS

The SCAPS-1D package was used to examine the structure of a PSC device made of Glass/FTO/ETM/MAPbI₃/Spiro-OMeTAD/Au. The effect of the MAPbI₃ layer thickness, carrier diffusion length, and band gap energy, as well as working temperature, was studied. The simulation results illustrate that: 1. the optimal thickness of the absorber layer is 500 nm, 2. the carrier diffusion length of the absorber layer should be higher than 2 μm to achieve high cell performance, 3. the engineering of the energy band gap is required to get high PCE of 25.40 %, and 4. the ZnO layer is a promising alternative ETM to TiO₂. The findings of this work are significant because they provide a deeper understanding of the operation mechanism and increase in the

efficiency of hybrid organic-inorganic perovskite-based fourth-generation solar cells.

ACKNOWLEDGEMENTS

The authors are grateful to Mr. Marc Burgelman from the University of Gent in Belgium for providing the SCAPS package.

REFERENCES

1. L. Et-taya, A. Benami, T. Ouslimane, *Sustainability* **14** No 3, 1916 (2022).
2. L. Et-taya, T. Ouslimane, A. Benami, *Sol. Energy* **201** No 1, 827 (2020).
3. J. Li, J. Duan, X. Yang, Y. Duan, P. Yang, Q. Tang, *Nano Energy* **80**, 105526 (2021).
4. T.C.-J. Yang, P. Fiala, Q. Jeangros, C. Ballif, *Joule* **2** No 8, 1421 (2018).
5. A. Kojima, K. Teshima, Y. Shirai, T. Miyasaka, *J. Am. Chem. Soc.* **131** No 17, 6050 (2009).
6. K.R. Adhikari, S. Gurung, B.K. Bhattarai, B.M. Soucase, *Physica status solidi c*, **13** No 1, 13 (2016).
7. Y. Raoui, H. Ez-Zahraouy, N. Tahiri, O. El Bounagui, S. Ahmad, S. Kazim, *Sol. Energy* **193**, 948 (2019).
8. T. Ouslimane, L. Et-taya, L. Elmaimouni, A. Benami, *Heliyon* **7** No 3, e06379 (2021).
9. A. Daraie, A. Fattah, *Opt. Mater.* **109**, 110254 (2020).
10. H.-J. Du, W.-C. Wang, J.-Z. Zhu, *Chin. Phys. B* **25** No 10, 108802 (2016).
11. H. Fujiwara, R.W. Collins, *Applications and Optical Data of Solar Cell Materials* 2 (Springer: 2019).
12. L. Huang, X. Sun, C. Li, R. Xu, J. Xu, Y. Du, Y. Wu, J. Ni, H. Cai, J. Li, Z. Hu, J. Zhang, *Sol. Energy Mater. Sol. Cells* **157**, 1038 (2016).
13. S. Sajid, A.M. Elseman, J. Ji, S. Dou, D. Wei, H. Huang, P. Cui, W. Xi, L. Chu, Y. Li, B. Jiang, M. Li, *Nano-Micro Lett.* **10** No 3, 51 (2018).
14. M. Shasti, A. Mortezaali, *Physica status solidi a* **216** No 18, 1900337 (2019).
15. T. Minemoto, M. Murata, *Journal of applied physics* **116** No 5, 054505 (2014).
16. Y. Kawano, J. Chantana, T. Nishimura, T. Minemoto, *Sol. Energy Mater. Sol. Cells* **205**, 110252 (2020).
17. S. Albrecht, M. Saliba, J.-P. Correa-Baena, K. Jäger, L. Korte, A. Hagfeldt, M. Grätzel, B. Rech, *Journal of Optics* **18** No 6, 064012 (2016).
18. M. Anaya, G. Lozano, M.E. Calvo, H. Míguez, *Joule* **1** No 4, 769 (2017).
19. M.-c. Kim, B.J. Kim, D.-Y. Son, N.-G. Park, H.S. Jung, M. Choi, *Nano Lett.* **16** No 9, 5756 (2016).

Порівняння впливу ZnO та TiO₂ на характеристики перовскітних сонячних елементів за допомогою програмного пакету SCAPS-1D

A. Benami¹, T. Ouslimane¹, L. Et-taya¹, A. Sohani²

¹ LMZER-O TEA, Department of Physics, Faculty of Sciences and Techniques, Moulay Ismail University of Meknes, BP 509 Boutalamine 52000, Errachidia, Morocco

² Lab of Optimization of Thermal Systems' Installations, Faculty of Mechanical Engineering-Energy Division, K.N. Toosi University of Technology, P.O. Box: 19395-1999, No. 15-19, Pardis St., Mollasadra Ave., Vanak Sq., Tehran 1999 143344, Iran

У пошуках високоефективного та недорогого матеріалу для фотоелектричних пристроїв четвертого покоління органічно-неорганічні гібридні перовскітні сонячні елементи набувають популярності як новий поглинач. Зараз досліджуються два типи архітектури твердотільних перовскітних пристроїв. Це мезопористі і плоскі гетеропереходи. Обидві структури складаються з п'яти шарів: прозорого провідного оксиду, матеріалу для переносу електронів, активного шару перовскіту, матеріалу для переносу дірок, і зворотного контакту. У роботі за допомогою одновимірного симулятора ємності сонячних елементів (SCAPS-1D) моделюються ключові характеристики перовскітних сонячних елементів з оксидом цинку (ZnO) та діоксидом титану (TiO₂) як матеріалом для переносу електронів. TiO₂ є найбільш часто використовуваним матеріалом в перовскітних сонячних елементах, але для його осадження потрібна висока температура, яка обмежує промислову обробку пристроїв. ZnO широко використовується в напівпровідниковій промисловості і вважається альтернативою TiO₂ завдяки відмінному переносу електронів. Дослідження за допомогою моделювання зосереджені на товщині, довжині дифузії носіїв та енергії забороненої зони шару поглинача, які впливають на фотоелектричні властивості пристроїв на сонячних елементах. Також досліджується вплив робочої температури. Згідно з результатами, використання ZnO як матеріалу для переносу електронів покращує ефективність сонячних елементів порівняно з TiO₂. Завдяки нижній межі зони провідності, яка полегшує перенос фотогенерованих електронів у перовскітному сонячному елементі, найкраща ефективність, отримана від структури з використанням шару ZnO, становить 25,40 % при температурі навколишнього середовища. Результати моделювання показують, що товщина поглинача 500 нм підходить для досягнення високої ефективності пристроїв.

Ключові слова: Перовскіт, Сонячні елементи, Ефективність, SCAPS-1D.